Ceramics International 44 (2018) 7746–7753

Contents lists available at ScienceDirect

Ceramics International

journal homepage: www.elsevier.com/locate/ceramint

Synthesis and properties of HA/ZnO/CNT nanocomposite

M. Ding[a], N. Sahebgharani[a], F. Musharavati[b], F. Jaber[c], E. Zalnezhad[a,*], G.H. Yoon[a]

[a] Department of Mechanical Convergence Engineering, Hanyang University, Seoul, Republic of Korea
[b] Mechanical and Industrial Engineering Department, College of Engineering, Qatar University, 2713 Doha, Qatar
[c] Department of Biomedical Engineering, Ajman University, United Arab Emirates

ARTICLE INFO

Keywords:
Hydroxyapatite
Zinc oxide
Carbon nanotube
Nanocomposite
Mechanical properties
Wear resistance

ABSTRACT

The goal of this study was to examine the tribomechanical properties of hydroxyapatite (HA)/ZnO and HA/ZnO/CNT composite ceramics (carbon nanotubes; with different ratios 0.5 wt%, 1.0 wt%, and 1.5 wt%). The composites were synthesized using the hydrothermal method in an autoclave. The structure and morphology of the composites were analyzed using Fourier transform infrared spectroscopy (FTIR), X-ray diffraction (XRD), energy-dispersive X-ray analysis (EDX) and transmission electron microscope (TEM). The consolidation process was performed by sintering the compounds at 1150 °C under an argon gas atmosphere. The effects of ZnO and CNT on the mechanical properties and wear resistance of the HA-nanoparticle-based ceramic composites were investigated using a Vickers hardness tester, nanoindentation, and reciprocating wear tester equipment. The nanohardness and elastic modulus of the sintered samples increased and the friction coefficient of the sintered samples decreased as the fraction of CNTs increased compared to the pure HA and HA/ZnO compounds. Furthermore, the wear loss of HA/ZnO/CNT composites decreased with the increase in the CNT content compared to the HA and HA/ZnO samples.

1. Introduction

Bone tissue engineering, which attempts to guide bone regeneration, is a promising way to correct bone defects caused by severe trauma, tumor resection, and congenital malformations. Nanotechnology offers a wide range of alternatives to design new biomaterials for bone tissue engineering application, endowing biomaterials with biocompatibility and excellent mechanical properties. Over the past decade, nanotechnology has been one of the fastest growing areas of science and technology. The extraordinary physical and chemical properties of various nanomaterials facilitate the creation of new structures, systems, platforms, and even devices with potential applications in a wide variety of disciplines.

The clinical success of implants is influenced by the biomaterial device integration with surrounding body tissues [1]. Along with the cellular interaction reassurance, the surface of biomaterials ought to discourage the adhesion of infectious bacteria, which is one of the main reasons for implant failure [2]. Polymethylmethacrylate (PMMA) along with antimicrobial agents have been utilized to prevent and treat orthopedic infections [3]. However, PMMA bone cement has numerous drawbacks, including thermal damage to the antibiotics, short duration of release, and biocompatibility reduction with bone [4]. Recently, studies have focused on inorganic antibacterial biomaterials to control bacteria [5]. Inorganic biomaterials have advantages, including durability, stability, and safety, in comparison with organic antibacterial biomaterials [6]. The most widely studied inorganic nanomaterials for biomedical applications include hydroxyapatite nanoparticles (nHA) [7] and zinc oxide (ZnO) nanomaterial [8]. Carbon nanotubes (CNTs), considered the stiffest and strongest of organic materials, have been significantly utilized in biomedical applications [9].

Calcium phosphate containing phosphate anions and calcium cations can be found in the form of pyrophosphates, orthophosphates, and metaphosphates [10]. It is also available as a dental product in dental chewing gums and toothpaste [11]. Hydroxyapatite (HA), a natural form of calcium phosphate, is the core component of teeth and bones. HA nanoparticles, with the chemical composition $Ca_{10}(PO_4)_6(OH)_2$ in pure stoichiometric form, have been a main topic of study in bone replacement due to their outstanding biocompatibility, along with their chemical composition, mechanical properties, and structure, which are identical to that of bone mineral [12]. To mimic bone mineral, mechanical and biological properties within bone tissue, HA is broadly utilized [13] as implants in artificial hard tissue replacement in maxillofacial, orthopedics, and dental implant surgery [14,15]. Due to its poor strength and brittle nature, HA has limited orthopedic applications in damaged bones. In the last few decades, to fabricate a similar biomaterial for prosthetic implants, research has been carried out to

* Corresponding author.
E-mail address: e.zalnezhad@gmail.com (E. Zalnezhad).

https://doi.org/10.1016/j.ceramint.2018.01.203
Received 3 January 2018; Received in revised form 23 January 2018; Accepted 24 January 2018
Available online 31 January 2018

develop HA-based composite material. It is known that nanomaterials with exclusive structures show superior biocompatibility and higher mechanical properties. Therefore, HA is fortified with the use of ceramic microfillers such as silicon carbide, alumina [17], zirconia [16], and titania [18]. HA nanoparticles with alumina and titania nanoceramics with large surface areas increase the proliferation and adhesion of osteoblasts [19]. Accordingly, nanoceramics with improved bioactivity enable implant integration with human tissues [20–23]. Nevertheless, due to the lack of antibacterial properties of HA-based composites, it remains an open problem that needs to be solved. Saha et al. [24] investigated the effect of ZnO in HA/ZnO biocomposites and found that ZnO had antibacterial effects against both gram-positive and gram-negative bacteria [25]. ZnO can be dissolved in a culture medium and release Zn^{2+} ions. It provides reactive oxygen species that play a significant role in constraining bacterial growth, forming a biofilm, and increasing bactericidal activity [26].

Zinc oxide has been widely used in many fields such as rubber, ceramics, textile, and cosmetics owing to its excellent physical, chemical, and biological properties. In recent years, its biomedical applications have received increasing attention. One of the most important features of ZnO nanomaterials is its non-toxicity. [27]. Stanić et al. [28] investigated the antibacterial property of Zn/HA in which zinc incorporation into HA showed that zinc replaces calcium in HA structures [29]. A study by Aina et al. on the reactivity of hydroxocarbonate apatite formation of bioglass was conducted, and they found that Zn produced an extreme decrease in the overall glass leaching activity. However, at 20% Zn concentration, the hydroxycarbonate apatite formation on the surface of the glass was completely constrained. ZnO with higher concentration in bioglasses inhibits the transformation of amorphous calcium phosphate to hydroxocarbonate apatite [30]. The activation of the particle surface leads to diverse performance during precipitation and dissolution [31]. Based on these desirable properties, ZnO nanomaterials have attracted immense interest in biomedical applications. Zhou et al. [32] reported the synthesis of a nanohydroxyapatite/zinc oxide complex via a precipitation process and investigated the antimicrobial properties composite. They found that Zn^{2+} ions of ZnO entered the n-HA crystal lattice and that the HA/ZnO composite had good antibacterial activity against Staphylococcus aureus and Escherichia coli with proper biocompatibility. The materials comprising an HA/ZnO system have immense potential for application of antibacterial biomaterials and for dental fillings and repairs.

Low fracture toughness, intrinsic brittleness, and insufficient wear resistance of the HA implants [33–39] have led to research focused on improving the biological and mechanical properties of composite ceramic materials. Chen et al. [40] studied the influence of CNTs on the mechanical properties of HA/CNT composite using nanoindentation tests. They concluded that HA/CNT composite with more CNTs had better properties. Zhao et al. [41] carried out compression tests on HA/CNT composites and found an increment in the compressive strength of HA. In their study, 2 wt% multi-wall carbon nanotubes in HA had a 38% enhancement in the strength of the composite.

Ioku et al. [42,43] studied the synthesis of porous HA ceramics using a hydrothermal technique at low temperature for bone generation. Lopu et al. [35] successfully prepared zirconia/CNT composite using a hydrothermal process.

The aim of this study was to synthesize HA/ZnO/CNTs with different CNT levels using a hydrothermal technique. SEM, XRD, TEM, and FT-IR were used to examine the structure and morphology of the composites. The tribomechanical properties of the composites were evaluated using nanoindentation, Vickers microhardness testing, and wear tester equipment.

2. Experimental methods

2.1. Materials

HA (purity ≥ 97%; < 100 nm particle size) and ZnO (puriss. p.a.; ACS reagent; ≥ 99.0%) powders were purchased from Aladdin Inc. and Sigma-Aldrich Inc., respectively. CNTs (type: single-walled CNT; weight: 1 g; grade: SA210; method: arc process) were purchased from Nano Solution Corporation.

2.2. Sample preparation

The compound HA/ZnO/CNT powder was prepared using the hydrothermal method. The ratio of HA and ZnO powders was 9:1, and subsequently, CNT powder was added to the HA/ZnO composite at different levels: 0.0, 0.5, 1.0, and 1.5 wt%. The mixture was dissolved in distilled water using ultrasonication for 1 h at room temperature (25 °C). Subsequently, the suspension was poured into an autoclave for a hydrothermal reaction at 180 °C for 8 h. The as-synthesized HA-ZnO samples with 0, 0.5, 1.0, and 1.5 wt% CNTs, named HA/ZnO, HA/ZnO/CNT0.5, HA/ZnO/CNT1.0, and HA/ZnO/CNT1.5, respectively, were separated centrifugally, rinsed four times with distilled water, and dried in a vacuum oven at 70 °C for 24 h.

To provide a disc for tribomechanical property investigation, the samples were uniaxially pressed at 250 MPa using a tungsten carbide die with diameter 5 mm. Then, the discs were sintered in a tube furnace at 1150 °C for 1 h in a highly pure argon gas atmosphere at a heating and cooling rate of 3 °C/min. Lastly, the sintered specimens were mounted with acrylic resin for assessing the tribomechanical properties. SiC paper (600, 1000, and 1800 grit) was used to polish the surfaces of the sintered composite discs.

2.3. Characterization

The morphological characterization and determination of particle size of the synthesized composite powders were performed using a transmission electron microscope (TEM, JEOL TEM2100F). To investigate the elemental composition of the specimens, an energy-dispersive X-ray analysis (EDX) attached to the TEM instrument was used. A PANalytical Empyrean X-ray diffraction (XRD) was utilized for structural analysis of the composites. Fourier transform infrared spectroscopy (FTIR) analyses were performed using a Thermo Scientific IS50 spectrophotometer to identify the functional group of the composites.

2.4. Mechanical property

The indentation method was conducted to analyze the mechanical properties of the sintered ceramic composite specimens. The nanoindentation tests (Micro materials Ltd., Wrexham, UK) were carried out to examine the nanohardness and the modulus of elasticity of the composites. Microhardness tests were conducted on composites using a Vickers hardness test machine (HMV, SHIMADZU Corporation, Japan). When the maximum penetration depth was reached, the loading was stopped, and then the load was maintained constant for 5 s. Microindentation tests were performed for four samples: 10 indentations were done for each sample with a load of 1.961 N, and the diamond scars were captured using an electron microscope to observe the indentation.

2.5. Tribological property

To study the tribological properties of the composite discs, a reciprocating wear test apparatus was used. Stainless steel balls with 4 mm diameters were used. Before the wear test, the composite discs and balls were rinsed in deionized water and acetone and dried with

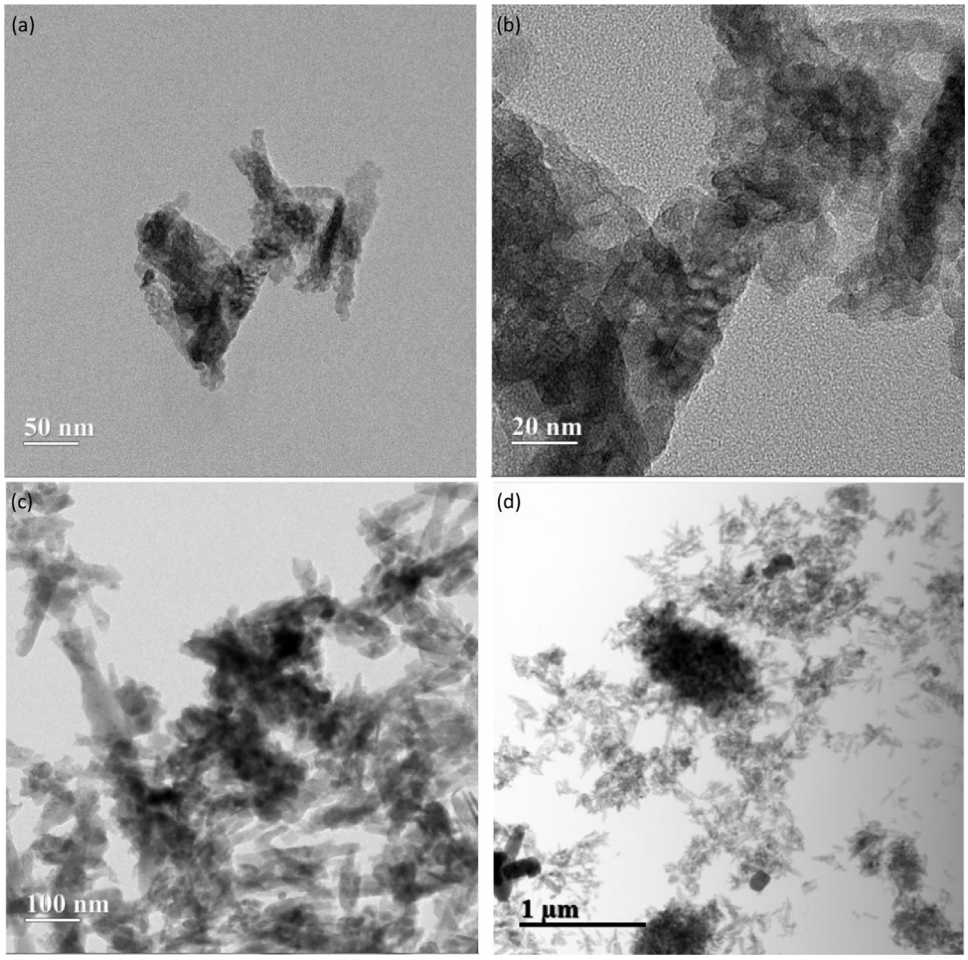

Fig. 1. TEM images of the HA/ZnO/CNT1.5.

nitrogen gas. During the wear testing, a reciprocating movement was created by an electro-motor. A normal load of 8.76 N was applied to the samples for the wear tests. The coefficient of friction (COF; μ_k) was revealed in the instrumentation output and calculated by F/N, in which F and N are the friction force and the normal force, respectively. To evaluate the wear loss, a high-precision (0.0001 mg) weight balance (METTER TOLEDO, Switzerland) was utilized.

3. Results and discussion

Fig. 1a–d show the TEM images of the HA/ZnO/CNT1.5 sample synthesized using the hydrothermal method. TEM micrographs illustrate the HA/ZnO complex particles. Fig. 2a–g show the EDX results of the composite, where the atomic ratio of Ca to P is observed to be approximately 1.5, which is consistent with the stoichiometric ratio of the nHA. Table 1 shows the EDX elemental composition of the composite.

The XRD patterns of the hydrothermally synthesized and sintered HA/ZnO and HA/ZnO/CNT1.5 ceramic composites are presented in Fig. 3. According to the XRD data in Fig. 3, the appearance of characteristic diffraction peaks of HA (PDF NO. 09–0432) located at 25.87°, 28.12°, 32.90°, and 39.20° corresponding to the (002), (102), (300), and (212) crystal planes, respectively, show that HA retained its hexagonal structure. Nevertheless, the wide peaks of HA are attributed to its poor crystallization [32]. On the other hand, the characteristic diffraction peaks of ZnO at 31.77°, 34.42°, 36.25°, and 47.53° corresponding to the (100), (002), (101), and (102) crystal planes, respectively, match the XRD pattern of ZnO powder (PDF NO. 36–1451). This suggests that a ZnO phase was formed in the complex. Furthermore, the characteristic diffraction peaks of CNTs at 22.76°, 29.31°, and 34.22° corresponding to the (120), (113), and (123) crystal planes were consistent with the data (PDF NO. 50–0926). Furthermore, the peaks of CNTs at 22.76° and 34.22° were dominated by HA and ZnO, respectively, and the peak of ZnO at 31.77° was dominated by HA.

FTIR was conducted to further investigate the existence and chemical state of carbon in the CNT-modified HA/ZnO composite powder. The FTIR spectra of the 1.5%-CNT-content-modified HA/ZnO, ZnO/HA, and pure HA are summarized in Fig. 4 (HA (a), HA/ZnO (b), and HA/ZnO/CNT1.5 (c)). It can be observed that the major bands of HA associated with PO_4^{3-} (1020, 962, 600, 604, and 560 cm^{-1}) and OH^- (3569 and 600 cm^{-1}) appeared, as seen in Fig. 4. The bands attributed to CO_3^{2-} (1418 and 1419 cm^{-1}) and HPO_4^- (873 cm^{-1}) also appeared in the spectra in Fig. 4 (HA, HA/ZnO, and HA/ZnO/CNT1.5). Kumar et al. [44] reported that B-type carbonate (CO_3^{2-}) for PO_4^{3-}-substituted HA was present in the composite. FTIR spectra also showed that there were some variations in the frequencies of PO_4^{3-} and OH^-, shifting to low wave numbers in the complex. Due to the low concentration of CNTs, no apparent peaks attributed to the characteristic stretching vibrations of C–C bonds related to the CNT modes were found in these FTIR spectra. Similar to graphite, CNT is normally relatively non-reactive, except at the nanotube caps, which are more reactive and have a tendency to oxidize and cause additional reactions due to the presence of dangling bonds [44].

Recent research has focused on mechanical properties such as the modulus of elasticity and nanohardness of ceramic composite materials using nanoindentation. Herein, the mechanical properties of the HA/ZnO compound and the compound with different ratios of CNT were determined.

The mechanical properties of the composites including microhardness, nanohardness, and elastic modulus were evaluated and their

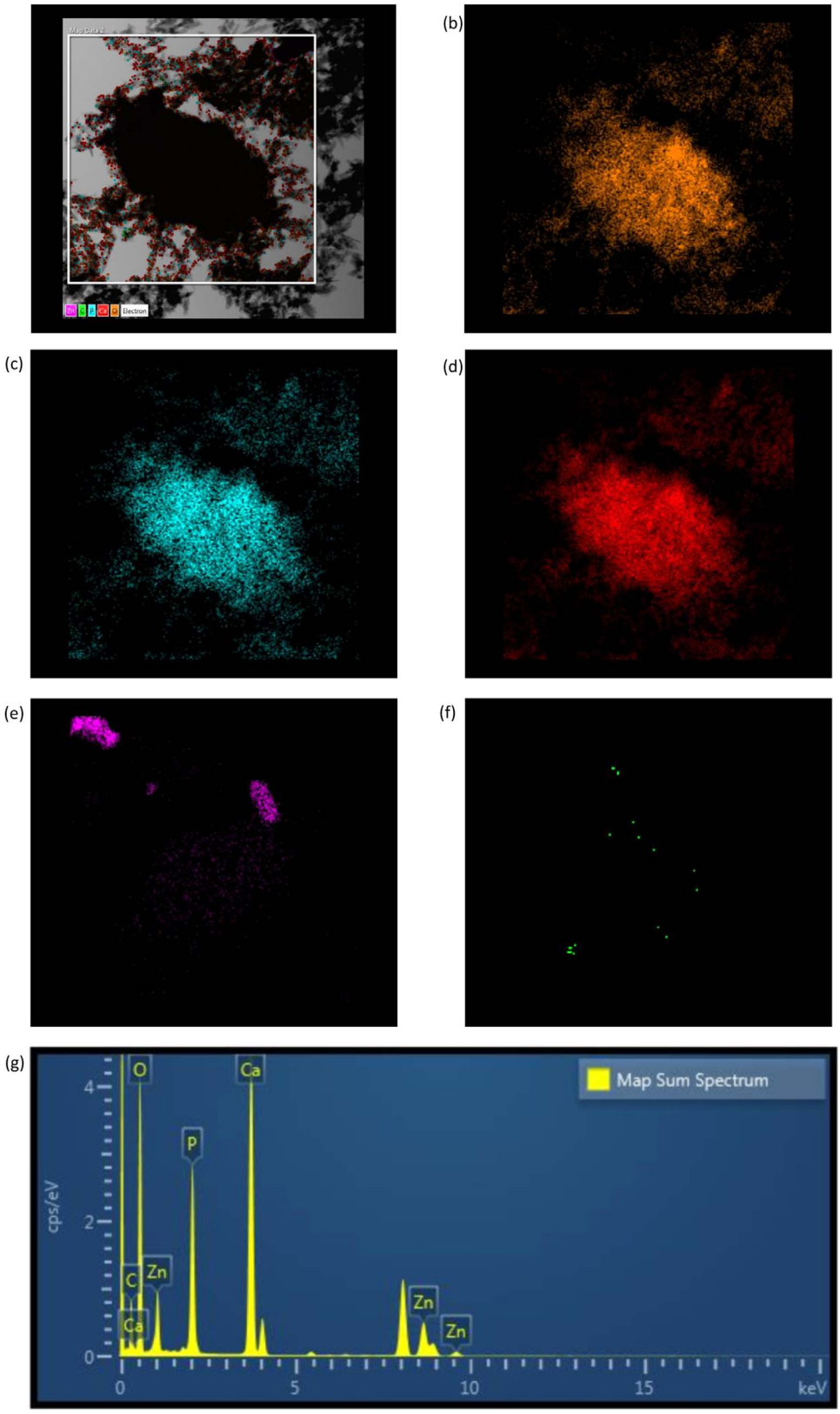

Fig. 2. EDX spectrum of HA/ZnO/CNT1.5.

summary is given in Table 2. Fig. 5a-c show the optical microscopy images of Vicker's hardness test indentation scars of HA/ZnO/CNT0.5, HA/ZnO/CNT1.0, and HA/ZnO/CNT1.5. Ten indentations were carried out for each sample and the average values are reported.

The microhardness values of the HA/ZnO/CNT composites increased as the CNT content increased from 0.5 to 1.5 wt% by approximately 141%, 155%, and 174%, respectively, compared to the pure HA sample. From the findings, it can be understood that even CNT with low concentrations has a major effect on the mechanical properties of composites. The increase in microhardness of the HA/ZnO/CNT1.5 composite depends on the residual porosity around the CNT after the sintering process.

Table 1
EDX elemental composition of the composite.

Element	Line Type	K Factor	Absorption Correction	wt%	wt% Sigma	Atomic%
C	K series	2.930	1.00	6.96	0.14	13.41
O	K series	2.133	1.00	35.57	0.15	51.48
P	K series	1.105	1.00	18.04	0.11	13.49
Ca	K series	1.008	1.00	34.23	0.12	19.77
Zn	K series	1.003	1.00	5.21	0.05	1.84
Total:				100.00		100.00

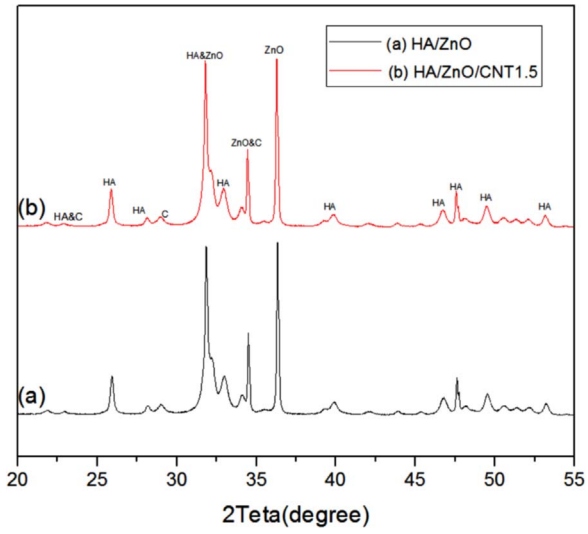

Fig. 3. XRD results of (a) HA/ZnO and (b) HA/ZnO/CNT1.5.

Notably, the nanohardness and elastic moduli can be obtained instantaneously as a function of depth. The influence of the content of CNT on the apparent elasticity modulus and nanohardness are investigated. Fig. 6(a), (c), (e) and (g) illustrate the nanohardness and elastic modulus of HA/ZnO, HA/ZnO/CNT0.5, HA/ZnO/CNT1.0, and HA/ZnO/CNT1.5 obtained by indentation at different depths ranging from 0 to 1000 nm. The average values of the nanohardness and elastic moduli of HA/ZnO were 0.943 GPa and 18.023 GPa, respectively. The average values of the nanohardness of the HA/ZnO/CNT0.5, HA/ZnO/CNT1.0, and HA/ZnO/CNT1.5 composites were 3.894 GPa, 4.227 GPa, and 5.206 GPa, respectively. The average values of the modulus of elasticity of the HA/ZnO/CNT0.5, HA/ZnO/CNT1.0, and HA/ZnO/CNT1.5 composites were 81.704 GPa, 85.022 GPa, and 92.836 GPa, respectively.

Fig. 6(b), (d), (f), and (h) show the normal load vs. penetration depth for the HA/ZnO, HA/ZnO/CNT0.5, HA/ZnO/CNT1.0, and HA/ZnO/CNT1.5 composites, respectively. The figures indicate an enhancement in the normal load with increasing penetration depth, whereas it decreases slightly beyond a depth of 1000 nm. It can be understood that during the indentation process, densification of CNT content and the wear of the dense surface were the two main processes of deformation and both happened beneath the indenter.

The nanohardness increased to shallow depths. However, after the nanohardness of the HA/ZnO reached 0.97 GPa (at a depth of 1000 nm), it decreased as the indentation depth increased. Similarly, Young's modulus of HA increased to 19.5 GPa and subsequently decreased slightly to 16.6 GPa. For the HA/ZnO/CNT0.5 composite, the nanohardness reached approximately 3.9 GPa at a depth of 342 nm and then decreased as the indentation depth increased. Likewise, the modulus of elasticity of the HA/ZnO/CNT0.5 composite was enhanced to 82.98 GPa at a penetration depth of 247 nm and then decreased somewhat to 74.64 GPa. The nanohardness of HA/ZnO/CNT1.0 at a depth of 365 nm was 4.2 GPa and afterward reduced with a further increase in the indentation depth. Also, the elastic modulus of HA/ZnO/CNT1.0 increased to 86.18 GPa at a depth of 388 nm and afterward decreased to 79.80 GPa. In the case of HA/ZnO/CNT1.5, the nanohardness and Young's modulus were 5.2 GPa at the depth of 199 nm and 93.58 GPa at the penetration depth of 301 nm and then decreased to lower values. This observation is expected to be due to the influence of CNT in HA/ZnO composites.

This result clarifies the reason that the areas beneath the indenter stylus involved both densifications and wear whereas the other areas were under shear stresses. Therefore, when the indenter stylus entered the composite material surface, the modulus of elasticity was improved because of the amplified contribution of CNT. Furthermore, the area densified close to the indentation scars had an insignificant influence on the material strength and caused wear between the indenter surface and the dense surface. The residual stress (hysteresis loop) rule for loading and unloading duration stipulates that the surfaces of a compound experience elastic energy dissipation, thereby creating larger compressive plastic deformation, stiffness, elastic response and frictional energy. Chen et al. employed nanoindentation technique to investigate the influence of the CNTs on mechanical properties of laser surface alloyed coatings. They found that the load increases with increasing content of carbon nanotube in the powder mixtures, which signifies that the more the content of CNT, the more the modulus of elasticity and nanohardness. Besides, after unloading, the plastic deformation of the coating without CNT and with CNT was about 1480 nm and 1290 nm for the HA–20% CNTs coating, respectively. This implies that HA without CNT experiences more plastic deformation during nanoindentation tests. Undoubtedly, CNT is one of the stiffest and strongest structures ever

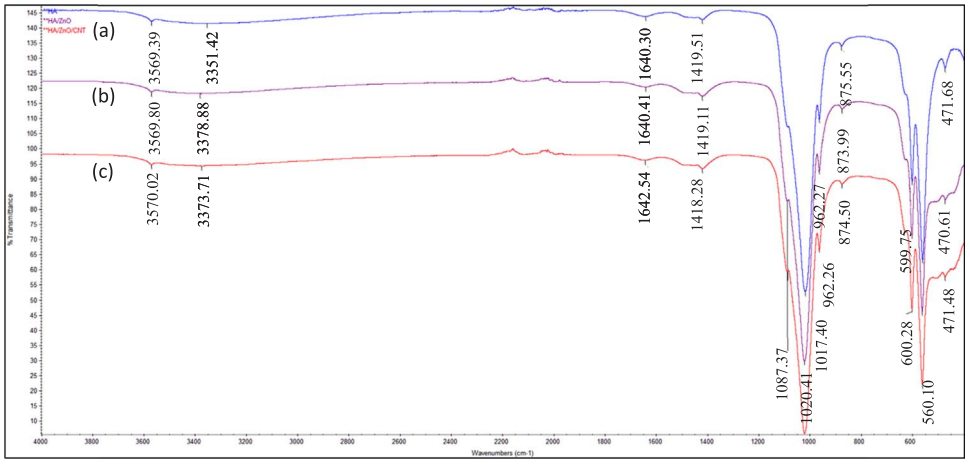

Fig. 4. FTIR spectra of (a) HA, (b) HA/ZnO, and (c) HA/ZnO/CNT1.5.

Table 2
Mechanical properties of the composites.

	Microhardness (Hv)	Nanohardness (GPa)	Elastic modulus (GPa)
HA	85.42	1.702	62.005
HA/ZnO	94.91	0.943	18.023
HA/ZnO/CNT0.5	206.1	3.894	81.704
HA/ZnO/CNT1.0	218.4	4.227	85.022
HA/ZnO/CNT1.5	235.7	5.206	92.836

made [45]. Thus, the residual CNTs and the in-situ formation of ZnO in the hydroxyapatite matrix, especially the residual CNTs, have a significant role in the strengthening of the composite. Usually, adding small content residual CNTs leads to the significant increase in the modulus of elasticity of the CNT reinforced hydroxyapatite based on the simple rule of mixtures [46].

It is evident that the nanohardness and modulus of elasticity are highly affected by the presence of CNT in the composite. In the composites of HA/ZnO/CNT, the elastic modulus of the composites with 1.0 wt% and 1.5 wt% CNT increased by 4% and 13% compared to that with 0.5 wt% CNT, respectively. The composite with the highest CNT content exhibited the largest nanohardness and elastic modulus among these samples. The enhancement of the modulus of elasticity of the compound was because of the greater value of elastic moduli related to the carbon reinforcement, a strong HA/C interface, and the uniform distribution of the CNT in the matrix [47]. From these consequences, it can be concluded that even at very low weight percentages, CNTs have a significant effect on strengthening and toughening the sintered HA/ZnO/CNT composite. Also, the mechanical properties can be influenced by the sintering process [48]. In the sintering procedure, Zhang et al. [49] identified improvements in the nanohardness, modulus elasticity, and fracture toughness of 43%, 61%, and 82%, respectively, in comparison with pure HA.

The wear test was conducted to investigate the tribological properties of the prepared nanocomposites containing different amounts of CNT. The tribological behaviors of HA, HA/ZnO, HA/ZnO/CNT0.5, HA/ZnO/CNT1.0, and HA/ZnO/CNT1.5 composites are indicated in terms of COF in Fig. 7.

It can be observed that CNT has a major influence on the COF of composites. The HA/ZnO disc exhibited the highest average COF and pure HA exhibited the second highest COF among all the samples. With the enhancement of the CNT content in the composites from 0 to 1.5 wt %, the composite appeared to have better wear resistance due to the increase in the surface hardness compared to the HA sample. The COF of the composites with CNT decreased by almost 50% compared to the pure HA and the HA/ZnO. The COF of HA/ZnO/CNT gradually decreased by almost 10% as the amount of CNT increased.

Fig. 8 shows the optical micrograph images (top views) of different samples after the wear test. The generation of the debris from the surface of the composite could be seen clearly with the necked eyes which were because of the reciprocating movement of the stainless steel ball under normal loading during the wear test. CNTs may play the role of a lubricator in the composites. This observation is consistent with the study by Lahiri et al. [46] wherein the COF of HA–CNT decreased during macro-wear due to the lubrication by delaminated graphene layers.

4. Conclusions

In this study, composites of HA/ZnO/CNT powder were synthesized using the hydrothermal method followed by a consolidation procedure by sintering the composites at 1150 °C. Compared to the pristine HA and compound HA/ZnO, the HA/ZnO/CNT composites exhibited improvements in mechanical properties. Vickers hardness and nanoindentation tests demonstrated that the sintered pure HA and HA composite bulks became much stronger with the inclusion of CNT. The nanoindentation results indicated that the nanohardness of the sintered HA/ZnO was 1/4 that of the sintered HA/ZnO/CNT0.5, and the elastic modulus of the sintered samples with the lowest CNT content increased four times compared to that of sintered HA/ZnO. The COF of the composites decreased significantly with the increase in CNT level from 0 to 1.5 wt%. Furthermore, the wear test results showed that CNTs had a significant influence on the reduction of wear loss during the reciprocating movement under a normal load.

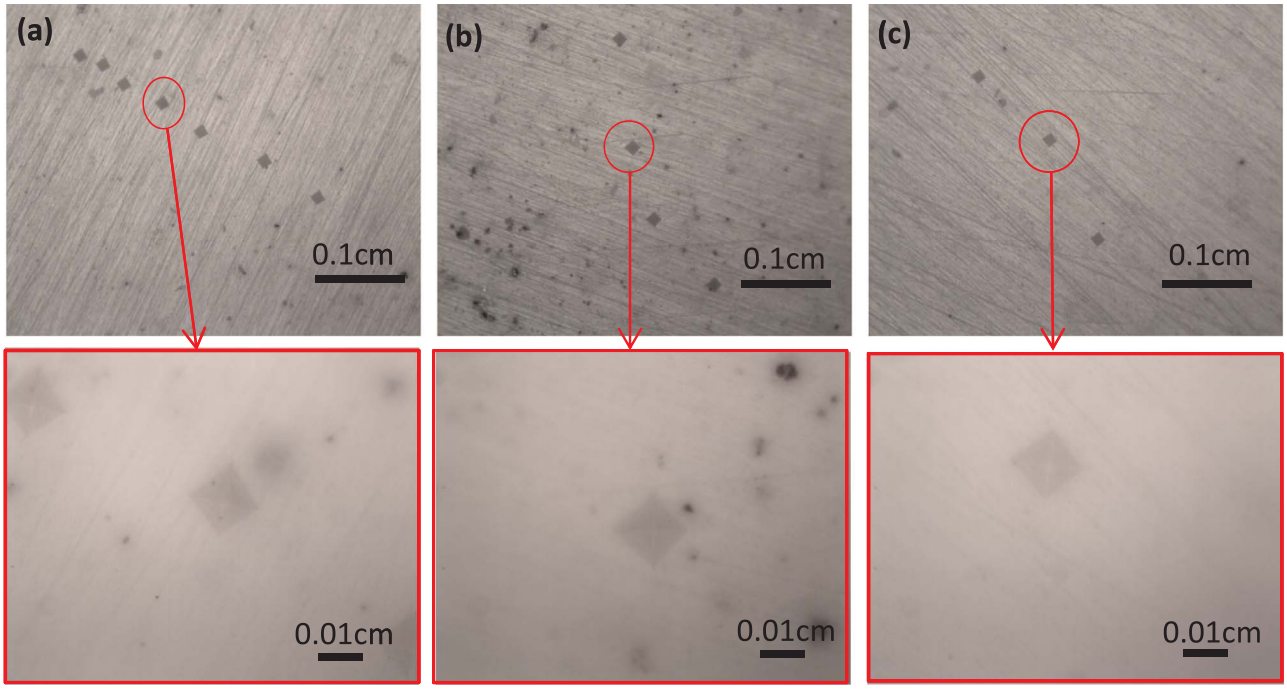

Fig. 5. Vicker's hardness test indentation scars of (a) HA/ZnO/CNT0.5; (b) HA/ZnO/CNT1.0; (c) HA/ZnO/CNT1.5.

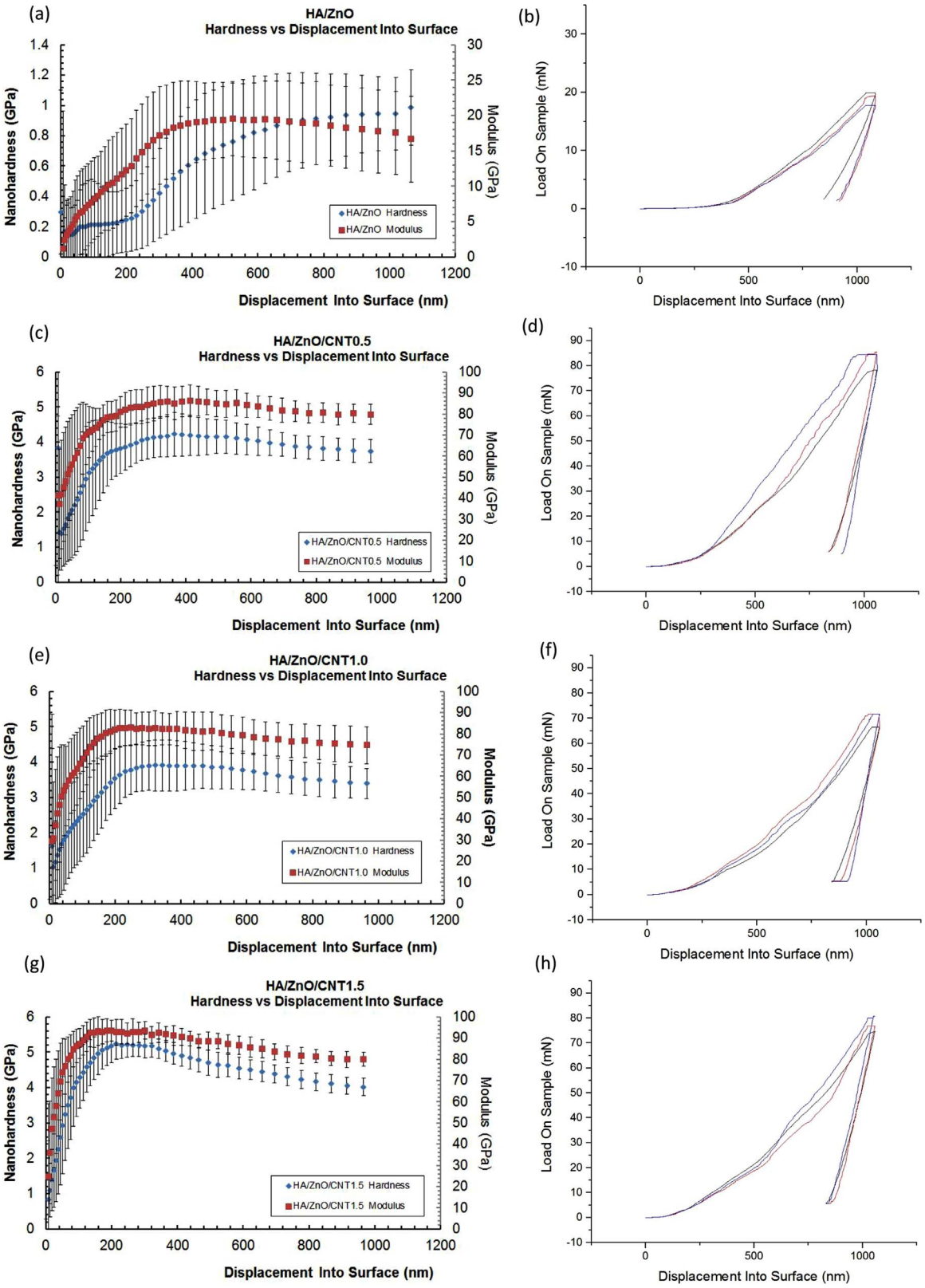

Fig. 6. Characteristic load vs nanoindentation depth for samples (a and b) HA/ZnO, (c and d) HA/ZnO/CNT0.5, (e and f) HA/ZnO/CNT1.0, and (g and h) HA/ZnO/CNT1.5.

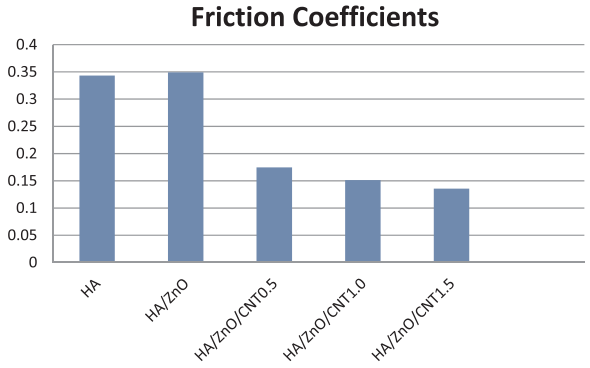

Fig. 7. Average friction coefficients (COF) for HA, HA/ZnO, and HA/ZnO/CNT for different CNT contents.

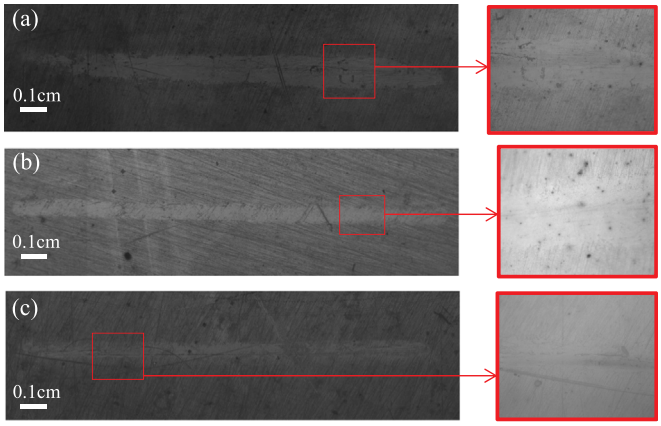

Fig. 8. Wear test with HA/ZnO/CNT (a) 0% (b) 0.5% (c) 1.0% (d) 1.5%.

Acknowledgement

We acknowledge Hanyang University's financial support through the Young Faculty Forum Fund (number 201600000001555). Also, some parts of the research were supported by the Fusion Research Program for Green Technologies through the National Research Foundation of Korea (NRF) funded by the Ministry of Science, ICT & Future Planning (No. NRF-2015R1A2A2A11027580).

References

[1] J. Cordero, L. Munuera, M. Folgueira, The influence of the chemical composition and surface of the implant on infection, Injury 27 (1996) S/C34–S/C37.
[2] M. Sarraf, et al., Effect of microstructural evolution on wettability and tribological behavior of TiO 2 nanotubular arrays coated on Ti–6Al–4V, Ceram. Int. 41 (6) (2015) 7952–7962.
[3] K.L. Garvin, A.D. Hanssen, Infection after total hip arthroplasty. Past, present, and future, JBJS 77 (10) (1995) 1576–1588.
[4] U. Joosten, et al., Evaluation of an in situ setting injectable calcium phosphate as a new carrier material for gentamicin in the treatment of chronic osteomyelitis: studies in vitro and in vivo, Biomaterials 25 (18) (2004) 4287–4295.
[5] M. Wilczynski, Anti-Microbial Porcelain Enamels, in: 62nd Porcelain Enamel Institute Technical Forum: Ceramic Engineering and Science Proceedings, Volume 21, Issue 5. Wiley Online Library, 2000.
[6] J. Sawai, Quantitative evaluation of antibacterial activities of metallic oxide powders (ZnO, MgO and CaO) by conductimetric assay, J. Microbiol. Methods 54 (2) (2003) 177–182.
[7] A.K. Gaharwar, N.A. Peppas, A. Khademhosseini, Nanocomposite hydrogels for biomedical applications, Biotechnol. Bioeng. 111 (3) (2014) 441–453.
[8] Y. Zhang, et al., Biomedical applications of zinc oxide nanomaterials, Curr. Mol. Med. 13 (10) (2013) 1633–1645.
[9] D.A. Rey, C.A. Batt, J.C. Miller, Carbon nanotubes in biomedical applications, Nanotech. L. Bus. 3 (2006) 263.
[10] J.-P. Bonjour, et al., Calcium-enriched foods and bone mass growth in prepubertal girls: a randomized, double-blind, placebo-controlled trial, J. Clin. Investig. 99 (6) (1997) 1287.
[11] M. Tung, F. Eichmiller, Dental applications of amorphous calcium phosphates, J. Clin. Dent. 10 (1 Spec No) (1999) 1–6.
[12] L. Hench, J. Jones, Biomaterials, Artificial Organs and Tissue Engineering, Elsevier, 2005.
[13] S.V. Dorozhkin, M. Epple, Biological and medical significance of calcium phosphates, Angew. Chem. Int. Ed. 41 (17) (2002) 3130–3146.
[14] E. Charrière, et al., Mechanical characterization of brushite and hydroxyapatite cements, Biomaterials 22 (21) (2001) 2937–2945.
[15] A. Slosarczyk, J. Białoskórski, Hardness and fracture toughness of dense calcium–phosphate-based materials, J. Mater. Sci.: Mater. Med. 9 (2) (1998) 103–108.
[16] W. Suchanek, M. Yoshimura, Processing and properties of hydroxyapatite-based biomaterials for use as hard tissue replacement implants, J. Mater. Res. 13 (1) (1998) 94–117.
[17] B. Viswanath, N. Ravishankar, Interfacial reactions in hydroxyapatite/alumina nanocomposites, Scr. Mater. 55 (10) (2006) 863–866.
[18] W. Que, et al., Hydroxyapatite/titania nanocomposites derived by combining high-energy ball milling with spark plasma sintering processes, J. Eur. Ceram. Soc. 28 (16) (2008) 3083–3090.
[19] T.J. Webster, et al., Enhanced functions of osteoblasts on nanophase ceramics, Biomaterials 21 (17) (2000) 1803–1810.
[20] R. Contro, et al., Searching for a functionally graded hydroxyapatite-Ti dental implant with reliable mechanical behaviour through numerical models, J. Biomech. 39 (2006) S204.
[21] A. Volceanov, E. Volceanov, S. Stoleriu, Hydroxiapatite-zirconia composites for biomedical applications, J. Optoelectron. Adv. Mater. 8 (2) (2006) 585.
[22] C. Zhang, et al., Nano-alumina/hydroxyapatite composite powders prepared by in-situ chemical precipitation, Ceram. Int. 42 (1) (2016) 279–285.
[23] E. Şahin, Synthesis and Characterization of Hydroxyapatite-Alumina-Zirconia Biocomposites, İzmir Institute of Technology, 2006.
[24] N. Saha, A.K. Dubey, B. Basu, Cellular proliferation, cellular viability, and biocompatibility of HA-ZnO composites, J. Biomed. Mater. Res. Part B: Appl. Biomater. 100 (1) (2012) 256–264.
[25] N. Saha, et al., Sintering, microstructure, mechanical, and antimicrobial properties of HAp-ZnO biocomposites, J. Biomed. Mater. Res. Part B: Appl. Biomater. 95 (2) (2010) 430–440.
[26] N. Padmavathy, R. Vijayaraghavan, Enhanced bioactivity of ZnO nanoparticles—an antimicrobial study, Sci. Technol. Adv. Mater. 9 (3) (2008) 035004.
[27] A. Nel, et al., Toxic potential of materials at the nanolevel, Science 311 (5761) (2006) 622–627.
[28] V. Stanić, et al., Synthesis, characterization and antimicrobial activity of copper and zinc-doped hydroxyapatite nanopowders, Appl. Surf. Sci. 256 (20) (2010) 6083–6089.
[29] Y. Tang, et al., Zinc incorporation into hydroxylapatite, Biomaterials 30 (15) (2009) 2864–2872.
[30] V. Aina, et al., Zinc-containing bioactive glasses: surface reactivity and behaviour towards endothelial cells, Acta Biomater. 5 (4) (2009) 1211–1222.
[31] M. Moldovan, et al., Structural and morphological properties of HA-ZnO powders prepared for biomaterials, Open Chem. 13 (1) (2015).
[32] G. Zhou, et al., Synthesis, characterization, and antibacterial activities of a novel nanohydroxyapatite/zinc oxide complex, J. Biomed. Mater. Res. Part A 85 (4) (2008) 929–937.
[33] R. Olivares, S. Rodil, H. Arzate, Osteoinduction properties of graphite-like amorphous carbon films evaluated in-vitro, Diam. Relat. Mater. 16 (10) (2007) 1858–1867.
[34] S. Iijima, Helical microtubules of graphitic carbon, Nature 354 (1991) 56–58.
[35] F. Lupo, et al., Microstructural investigations on zirconium oxide–carbon nanotube composites synthesized by hydrothermal crystallization, Carbon 42 (10) (2004) 1995–1999.
[36] E.E. Keller, W.W. Triplett, Iliac bone grafting: review of 160 consecutive cases, J. Oral. Maxillofac. Surg. 45 (1) (1987) 11–14.
[37] Y. Gu, K. Khor, P. Cheang, Bone-like apatite layer formation on hydroxyapatite prepared by spark plasma sintering (SPS), Biomaterials 25 (18) (2004) 4127–4134.
[38] L.-G. Yu, et al., Effect of spark plasma sintering on the microstructure and in vitro behavior of plasma sprayed HA coatings, Biomaterials 24 (16) (2003) 2695–2705.
[39] K. Balani, et al., Tribological behavior of plasma-sprayed carbon nanotube-reinforced hydroxyapatite coating in physiological solution, Acta Biomater. 3 (6) (2007) 944–951.
[40] Y. Chen, et al., Carbon nanotube reinforced hydroxyapatite composite coatings produced through laser surface alloying, Carbon 44 (1) (2006) 37–45.
[41] L. Zhao, L. Gao, Novel in situ synthesis of MWNTs-hydroxyapatite composites, Carbon 42 (2) (2004) 423–426.
[42] S.C.J. Loo, et al., Synthesis and hydrothermal treatment of nanostructured hydroxyapatite of controllable sizes, J. Mater. Sci.: Mater. Med. 19 (3) (2008) 1389–1397.
[43] K. Ioku, et al., Hydrothermal preparation of tailored hydroxyapatite, J. Mater. Sci. 41 (5) (2006) 1341–1344.
[44] E.V. Basiuk, et al., Direct solvent-free amination of closed-cap carbon nanotubes: a link to fullerene chemistry, Nano Lett. 4 (5) (2004) 863–866.
[45] M.M.J. Treacy, T.W. Ebbesen, J.M. Gibbson, Exceptionally high young modulus observedfor individual carbon nanotubes, Nature 381 (1996) 678–680.
[46] Y. Chen, a., Y.Q. Zhang, T.H. Zhang, C.H. Gan, C.Y. Zheng, G. Yu, Carbon nanotube reinforced hydroxyapatite composite coatings produced through laser surface alloying, Carbon 44 (2006) 37–45.
[47] D. Lahiri, et al., Carbon nanotube toughened hydroxyapatite by spark plasma sintering: microstructural evolution and multiscale tribological properties, Carbon 48 (11) (2010) 3103–3120.
[48] Y. Zhao, et al., Microstructure and anisotropic mechanical properties of graphene nanoplatelet toughened biphasic calcium phosphate composite, Ceram. Int. 39 (7) (2013) 7627–7634.
[49] L. Zhang, et al., A tough graphene nanosheet/hydroxyapatite composite with improved in vitro biocompatibility, Carbon 61 (2013) 105–115.